Electronic Supplementary Material (ESI) for Lab on a Chip.

Supplementary Information

A disposable acoustofluidic chip for nano/micro particle separation using unidirectional acoustic transducers

Shuaiguo Zhao, Mengxi Wu, Shujie Yang, Yuqi Wu, Yuyang Gu, Chuyi Chen, Jennifer Ye, Zhemiao Xie, Zhenhua Tian, Hunter Bachman, Po-Hsun Huang, Jianping Xia, Peiran Zhang, Heying Zhang, and Tony Jun Huang*

Department of Mechanical Engineering and Materials Science, Duke University, Durham, NC 27708, USA

*To whom correspondence should be addressed: tony.huang@duke.edu

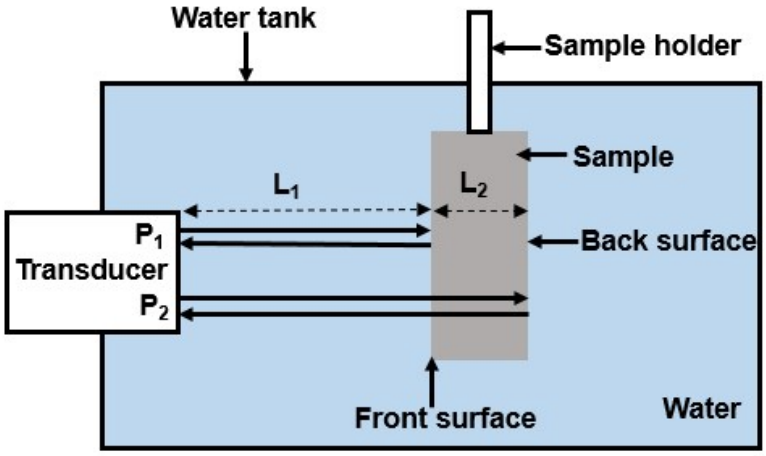

Fig. S1 A schematic diagram of the experimental setup for acoustic performance measurement. A sample with a thickness of L_2 is submerged in water. One transducer facing the sample at a known distance of L_1 excites an acoustic wave and receives its reflection from the back and front surface of the sample.

In **Fig. S1**, P_1 and P_2 are the amplitude of a frequency component for reflected acoustic waves from the front and back surface of the sample, respectively. Their dependence on physical parameters can be expressed by **Eq. 1**.

$$P_2 = P_1 T_1 T_1^* \frac{R_2}{R_1} e^{-2\alpha L_2} \quad (1)$$

Where, T_1, T_1^* are the transmission coefficients at the front surface from water to sample and from sample to water, respectively. R_1, R_2 are the reflection coefficient at the front surface from water to sample, and at the back surface from sample to water, respectively. T_1, T_1^*, R_1, and R_2 can be obtained through the acoustic impedance of water and sample. The frequency-dependent longitudinal wave speed (C_L) in the sample can be calculated based on the following **Eqs. 2** and **3**.

$$\varphi_1 = \varphi_0 - 2\pi f \frac{2L_1}{C_0} \quad (2)$$

$$\varphi_2 = \varphi_0 - 2\pi f \frac{2L_1}{C_0} - 2\pi f \frac{L_2}{C_L} \quad (3)$$

Here, φ_1, φ_2 are the phase of a frequency component for reflected acoustic waves from the front and back surface of the sample, respectively. φ_0, and C_0 are the initial phase and speed of the sound wave in water. By applying a Fourier Transform and analysis via a Matlab program, the acoustic attenuation of the sample at different frequencies and speeds of sound for a given sample can be obtained, shown in **Table 1**. Since the relationship between acoustic attenuation coefficient and frequency can be expressed by power function,[1, 2] **Eqs. 4** and **5** can be obtained by fitting the data in **Table 1** to power function based curve.

$$\alpha_{hard} = \pi r^2 = 0.59 f^{1.226} + 1.203 \quad (4)$$

$$\alpha_{soft} = 2.016f^{1.363} \quad (5)$$

Based on **Eqs. 4** and **5**, the acoustic attenuation coefficient of hard PDMS and soft PDMS at different frequencies can therefore be calculated, which is approximately 4432 dB/m for hard PDMS, and 23798 dB/m for soft PDMS at the frequency of 33.13 MHz.

Table 1 Acoustic performance comparison between "hard PDMS" and "soft PDMS".

Material	Speed of sound (m/s)	Acoustic attenuation coefficient (dB/cm)				
		1 MHz	2 MHz	3 MHz	4 MHz	5 MHz
"Hard PDMS"	1166 m/s	1.8	2.6	3.5	3.8	4.4
"Soft PDMS"	996 m/s	2.0	5.3	9.2	12.9	18.3

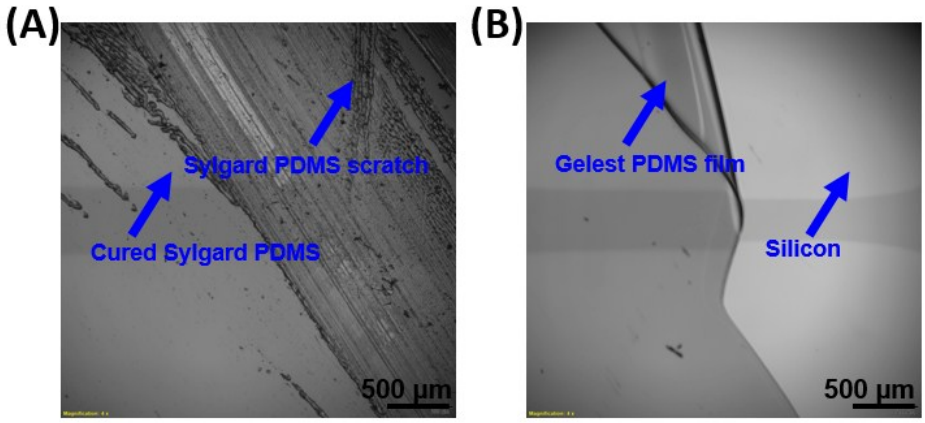

Fig. S2 The failure of fabricating PDMS film at a 1:1 ratio using common Sylgard 184 PDMS. PDMS films were fabricated at a 1:1 ratio of PDMS base to curing agent using (A) Sylgard 184 PDMS and (B) Gelest hPDMS. The results show that we could not peel off the cured Sylgard PDMS from silicon wafer at a mixing ratio of 1:1, and eventually Sylgard PDMS on the wafer was left with a scratch.

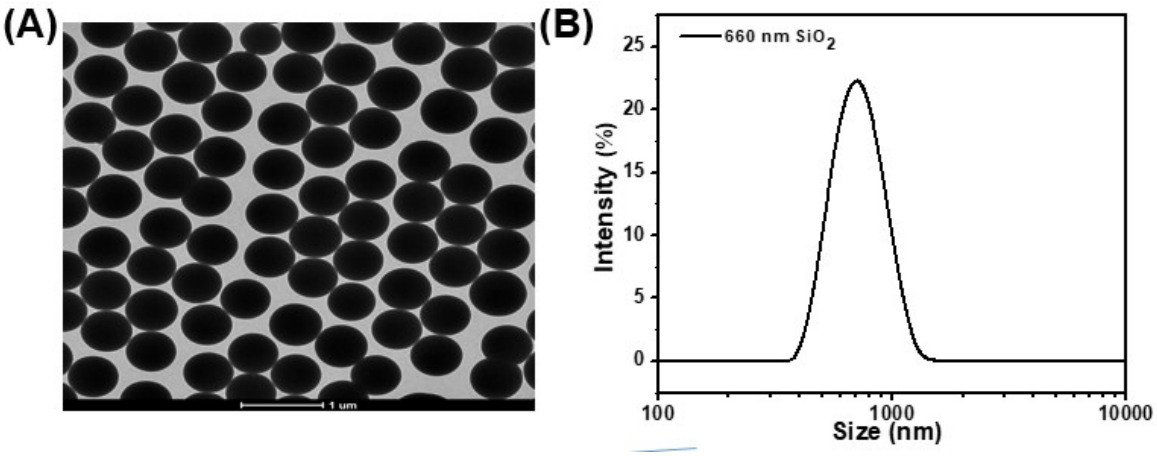

Fig. S3 Characterization of silicon dioxide (SiO_2) nanoparticles by (A) transmission electron microscope (TEM) and (B) Malvern zetasizer.

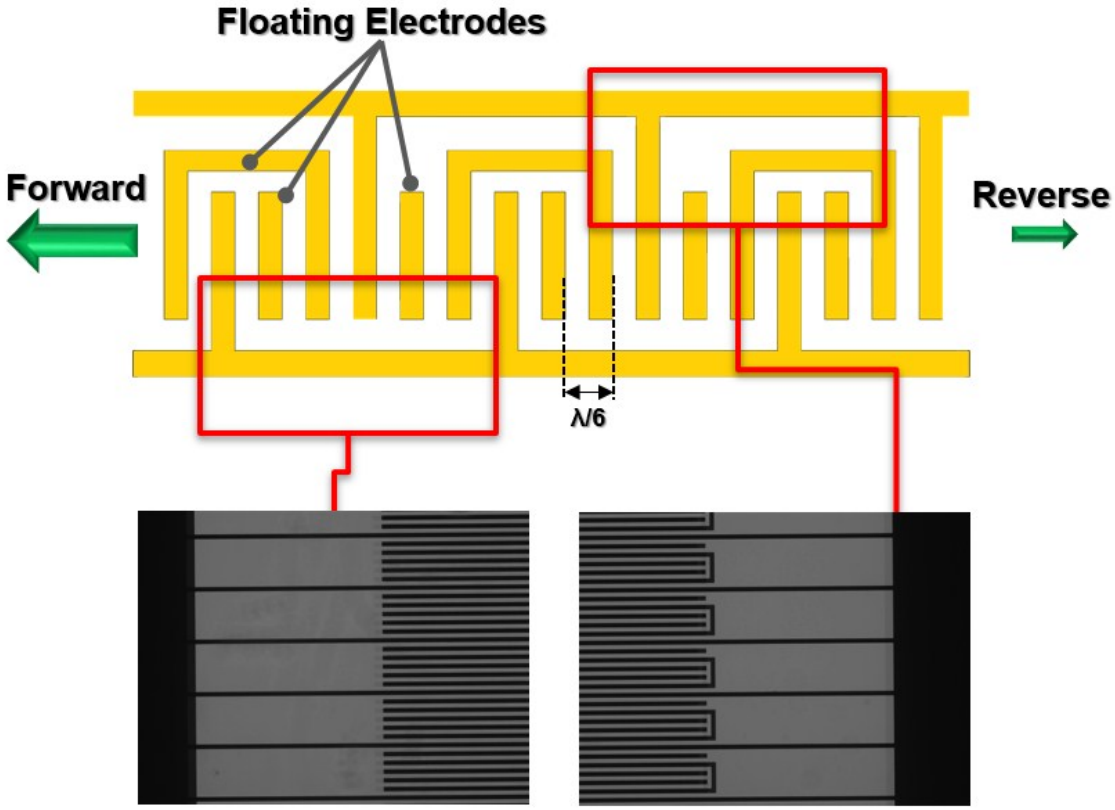

Fig. S4 The unidirectional interdigital transducer (IDT) design with floating electrodes. The floating electrodes increase the intensity of the forward wave by decreasing the reverse Rayleigh-mode surface acoustic waves (SAWs).

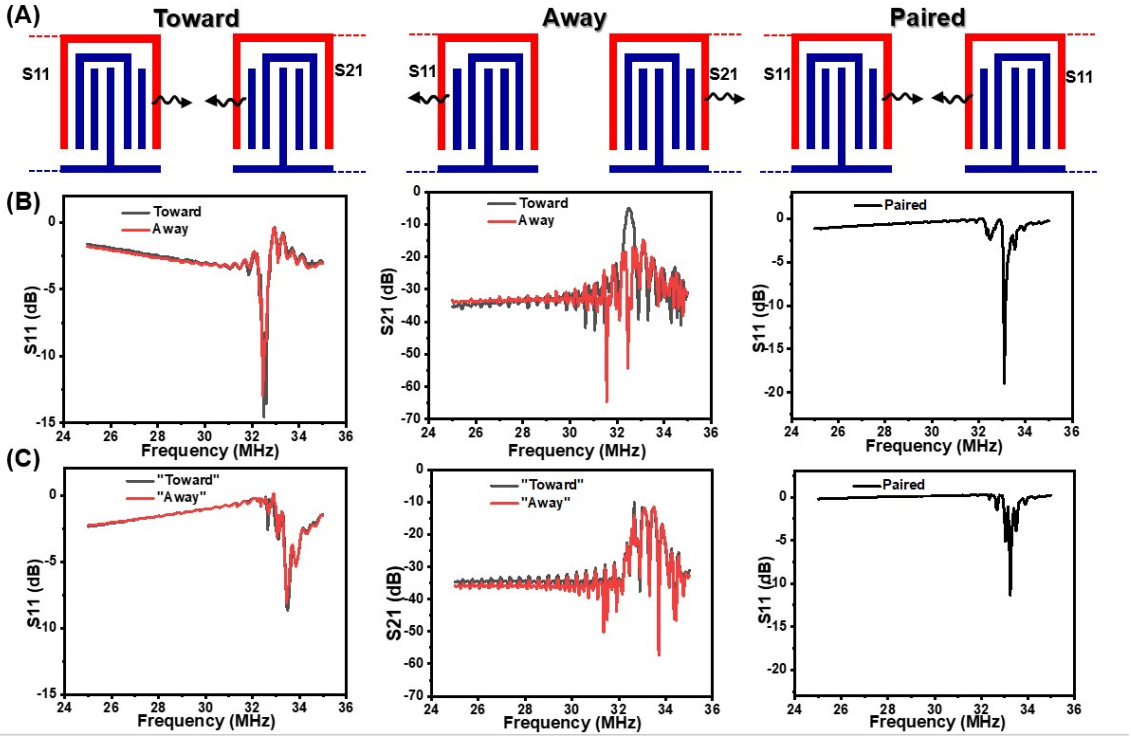

Fig. S5 Comparison of unidirectional IDT and bidirectional IDT. (A) Schematic toward, away, and paired IDT configurations for the reflection S11 and transmission S21 measurements. Here, "toward" configuration means that two identical SAWs propagate toward each other, while "away" configuration means that two identical SAWs propagate against each other. For both "toward" and "away" configurations, one side of the IDTs is measured as S11 and the other side is measured as S21. "Paired" configuration means that a pair of IDTs are connected together and both measured as S11. (B) Unidirectional IDT response as a function of frequency, for the "toward", "away" and "paired" configurations. (C) Bidirectional IDT response as a function of frequency, for the "toward", "away" and "paired" configurations. For comparison, the bidirectional IDT are simply designed in an inverse layout for the "toward" and "away" configurations. The results show that the unidirectional IDT has a smaller S11 than the bidirectional IDT at the resonance frequency in all three configurations, suggesting a weaker reflection and a stronger resonance effect. More importantly, the unidirectional IDT has a much larger S21 in the "toward" configuration relative to the "away" configuration, while the bidirectional IDT has almost equal S21 in the "toward" and "away" configurations, demonstrating the directionality of our unidirectional IDT. Specifically, the peak value of the S21 in (B) is ca. -5 dBm in the "toward" configuration and is only ca. -11.2 dBm in (C), indicating that the unidirectional IDTs can generate SAWs with higher amplitudes than traditional bidirectional IDTs. Note that the resonance frequency in the "toward" and "away" configurations is ca. 32.5 MHz, which shifts slightly from the center resonance frequency (ca. 33.13 MHz) in the "paired" configuration. Similar phenomenon has been reported in previous research, where the resonance frequency of IDTs shifts from 4.972 GHz to 4.785 GHz.[3] This frequency shift is ascribed to a series resistance and the stray capacitive coupling between IDTs,[3] but it would not affect experimental demonstrations since the IDTs are connected in a "paired" configuration to form standing surface acoustic waves during separation tests.

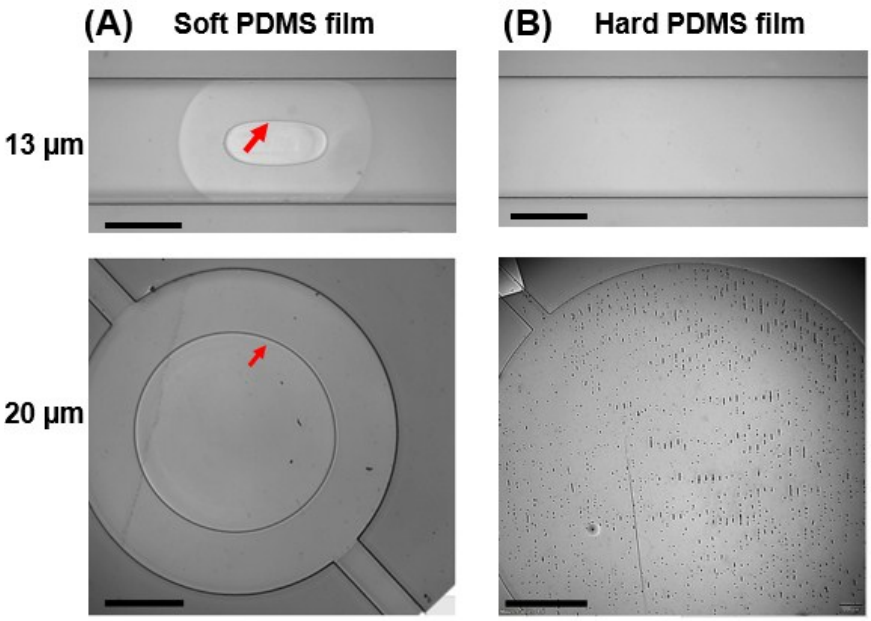

Fig. S6 Comparison of disposable microchannels fabricated by bonding a soft PDMS cavity to (A) soft PDMS film and (B) hard PDMS film, respectively. The soft PDMS film often adheres to the PDMS cavity and blocks the microchannel at both film thickness of 13 and 20 µm, represented by the red arrows. Conversely, the hard PDMS film is able to successfully enclose both the small rectangular and large circular PDMS cavity.

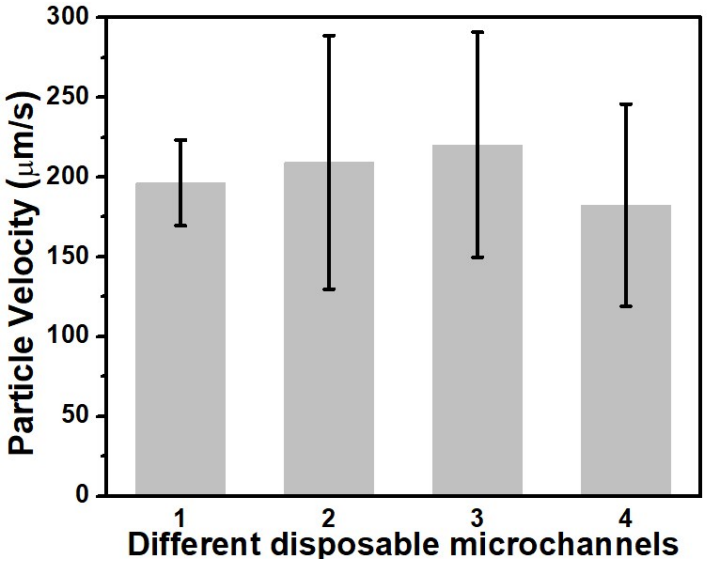

Fig. S7 Particle velocity measurement for 10 µm particles during their patterning within four different disposable hard/soft PDMS microchannel at a drive voltage of 20 V_{PP}.

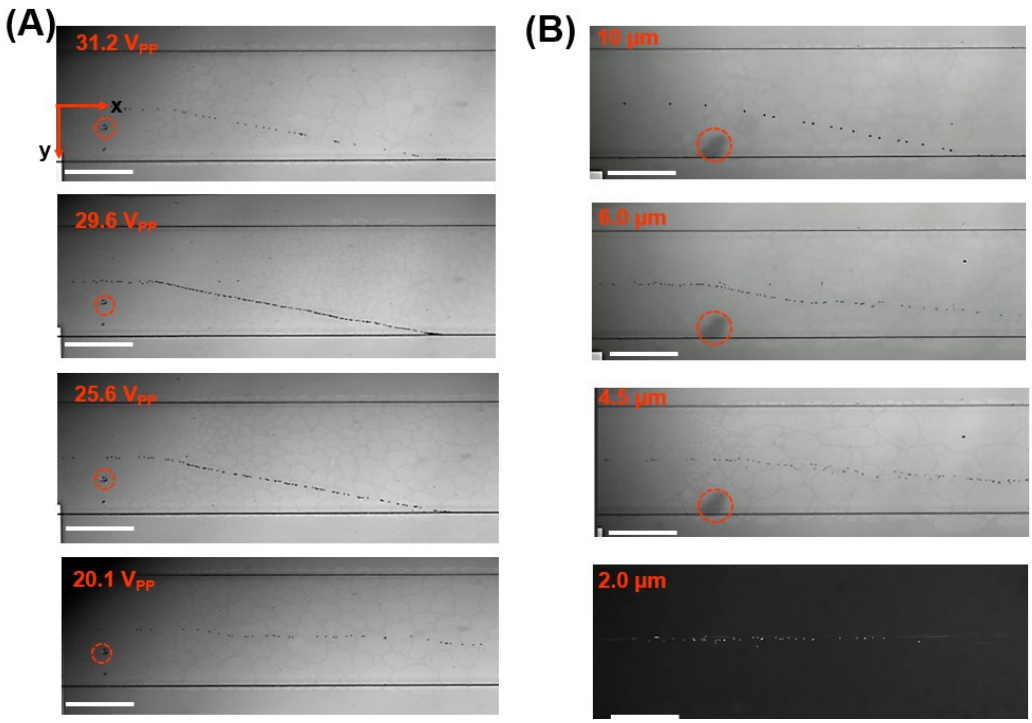

Fig. S8 Disposable acoustofluidic chips for particle deflection. (A) Deflection of 6 µm polystyrene (PS) particles at different acoustic intensities. (B) Deflection of different PS particles at the same acoustic intensity. Scar bar: 500 µm.

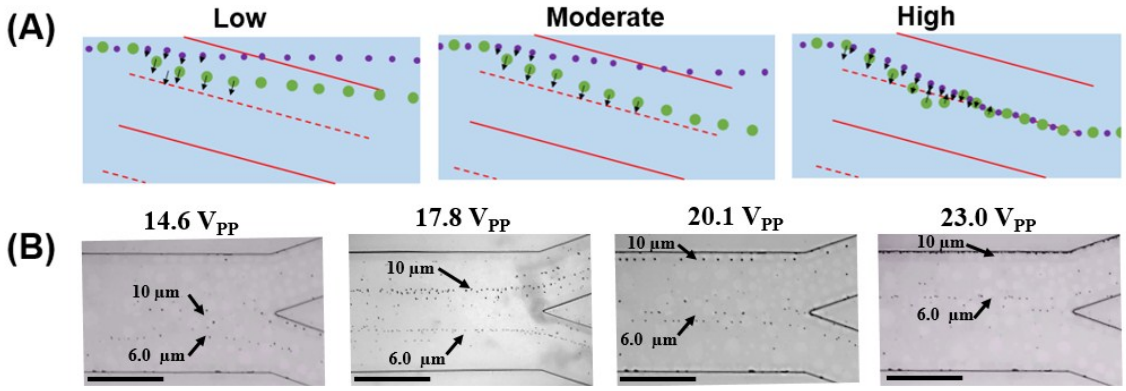

Fig. S9 (A) Schematic for the influence of acoustic intensity on particle separation. With increasing acoustic intensity, the difference in separation displacement would first increase and then decreases. (B) Experimental results show that the separation displacement for 6 and 10 µm PS particles first increases and then decreases with an increment in input power from 14.6 V_{PP} to 23 V_{PP}. Scale bar: 500 µm.

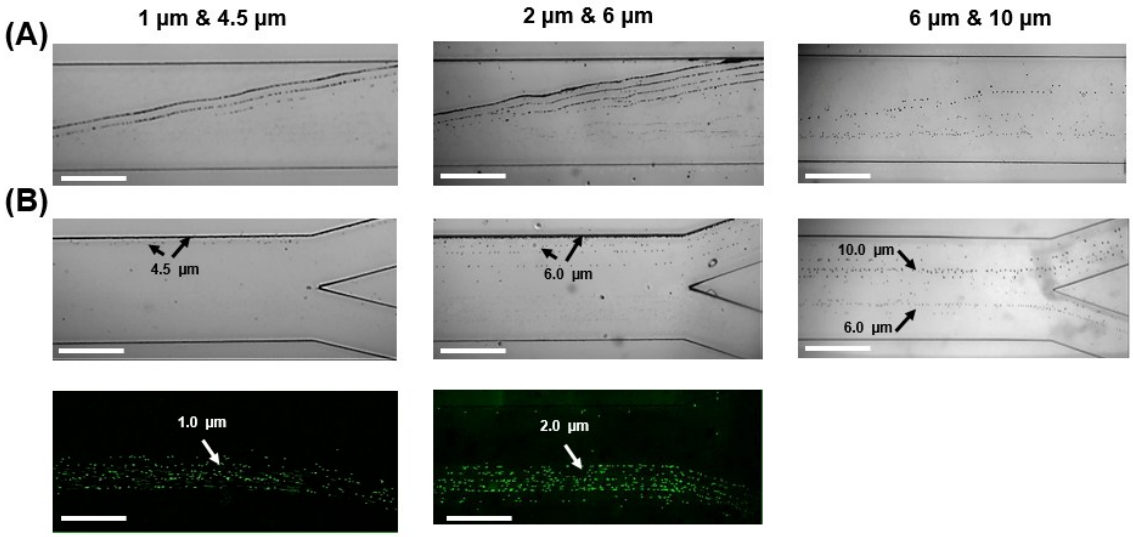

Fig. S10 Disposable acoustofluidic chips for separating mixtures of different PS microparticles. (A) The deflection of large particles at working regions with SAWs. The input power was 25.6 V_{PP}, 22.0 V_{PP}, and 17.8 V_{PP} for separating 4.5 μm, 6 μm, and 10 μm PS particles, respectively. (B) Bright-field and fluorescent images show the separated particles at the outlet region. Scale bar: 500 μm.

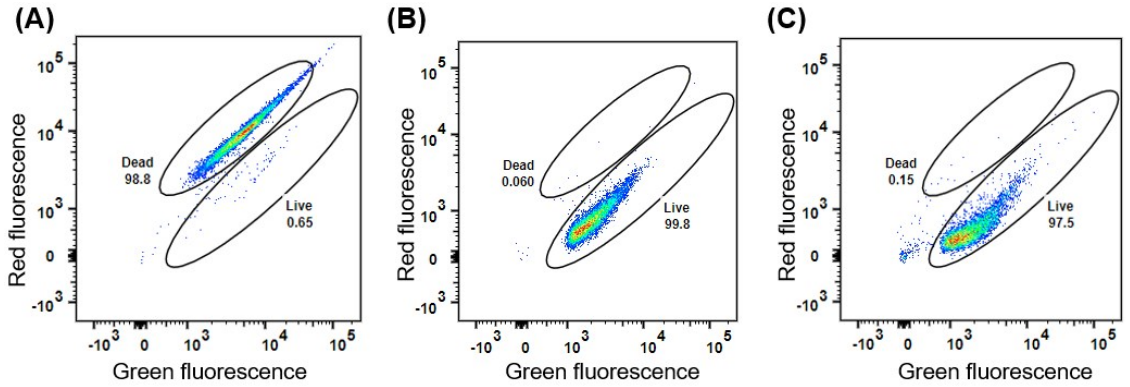

Fig. S11 Green fluorescence (SYTO 9, a membrane permeable stain) and red fluorescence (PI, a membrane impermeable stain) plot of cultured *E. coli* mixtures with different treatments: (A) viability after treatment in 70% isopropyl alcohol (IPA) for 30 mins as the control group: 0.65%, (B) viability before acoustic separation: 99.8%, and (C) viability after acoustic separation: 97.5 %. The bacteria viability of 97.5% after acoustic separation is almost identical to the viability before acoustic separation, demonstrating the biocompatibility of our disposable acoustofluidic devices.

Video Caption:

Video S1: 6 µm PS particles are separated at a high flow rate of 6 µL/min+6 µL/min+18 µL/min.

Video S2: 1 µm PS particles remained in the sample stream.

Video S3: 660 nm SiO_2 nanoparticles are deflected laterally, and separated from the 400 nm PS particles.

Video S4: 400 nm PS are slightly deflected and remained in the sample stream.

Video S5: Human RBCs were deflected accordingly, following a taSSAW field of ON-OFF-ON.

Video S6: *E. coli* bacteria remained in the sample stream.

References:

1. Z. Ni, C. Yin, G. Xu, L. Xie, J. Huang, S. Liu, J. Tu, X. Guo and D. Zhang, *Lab Chip*, 2019, 19, 2728-2740.

2. A. Thouvenot, T. Poepping, T. M. Peters and E. C. Chen, *International Society for Optics and Photonics*, 2016, 97835E.

3. É. Dumur, K. J. Satzinger, G. A. Peairs, M.-H. Chou, A. Bienfait, H.-S. Chang, C. Conner, J. Grebel, R. Povey and Y. Zhong, *Appl. Phys. Lett.*, 2019, **114**, 223501.